

## Contact with Friction Between 3D Beams with Deformable Circular Cross-Sections

Olga KAWA, Przemysław LITEWKA

*Institute of Structural Engineering  
Poznań University of Technology*

Piotrowo 5, 60-965 Poznań, Poland  
e-mail: {olga.kawa, przemyslaw.litewka}@put.poznan.pl

In this paper, contact with friction between three-dimensional elastic beams with deformations at the contact zone is analysed. It is assumed that the analysed beams undergo large displacements, although the strains remain small and the cross-sections of the beams are deformed. To include the deformation effect the classical analytical result from Hertzian contact between two elastic cylinders is used [3]. The penalty method is applied to enforce normal contact and friction constraints and the appropriate kinematic variables are defined, linearised and discretised for the finite element method implementation.

**Key words:** contact, beams, finite element method, friction, linearisation, deformed cross-section.

### 1. INTRODUCTION

The main purpose of computational contact mechanics is to provide numerical tools to properly describe the physical behaviour of bodies coming in contact, and especially the deformation and forces acting in the vicinity of contact interfaces.

Beam-to-beam contact is a special case of interaction between 3D bodies. There are several publications which are related to this subject, e.g., [2, 3, 6–8, 11, 13, 14]. The present paper reports an attempt to include cross-section deformations in the geometrical analysis of contact zones to improve the force-deformation relation.

A similar approach, for which contact stress and deformation are calculated using the Hertz theory, can be found in [11]. The nonlinear problem of contact interaction is solved by special iteration procedure using augmented technique with linearization, however this is limited to friction with small sliding.

The purpose of the present analysis is to investigate the influence of the Hertzian improvement of normal contact interface law on the results obtained in the frictional case of beam-to-beam contact.

A formulation for frictionless contact between beams in 3D space was proposed in [5]. We begin by using the results obtained in [5] to complete the formulation by adding contributions due to friction presented in [8]. The frictional law is restricted to the case of Coulomb friction. The classical solution of Hertzian contact between two cylinders [12] representing the contacting beams is used to improve the definition of the normal gap as in [5] and its influence on the frictional case is reported. Section 2 of this paper presents this classical solution and its consequences for the contact formulation presented in [8]. Also, for the sake of consistency, the details of the friction treatment detailed in [8] are given. In Sec. 3 several numerical examples are solved and in Sec. 4 some final remarks are presented.

## 2. KINEMATIC RELATIONS

### 2.1. Introduction

We consider two beams with circular cross-sections coming into contact. To detect a contact we have to define the penetration function which for beams with circular cross-sections can be written as

$$(2.1) \quad g_N = d_n - r_m - r_s + d,$$

where  $d_n$  is the minimum distance between the centre lines of the beams,  $r_m$  and  $r_s$  are radii of the beam cross-sections and  $d$  is the decrease of the radii due to deformation of the cross-section. To determine  $d_n$  we have to find a pair of two closest points lying on the axes of the beams ( $m$  and  $s$ ). Then the function of penetration can be used to define the contact criterion, which is defined as

$$(2.2) \quad g_N = d_n - r_m - r_s + d \leq 0.$$

### 2.2. Contact points

The location of the closest points  $C_{mn}$  and  $C_{sn}$  on the curves in 3D space is defined by local curvilinear co-ordinates:  $\xi_m$  for first beam and  $\xi_s$  for the second (Fig. 1). In the global Cartesian system  $(x_1, x_2, x_3)$  each point on a curve is associated with the position vectors  $\mathbf{x}_m$  and  $\mathbf{x}_s$ . These vectors correspond to the current beam configurations and can be expressed as

$$(2.3) \quad \begin{aligned} \mathbf{x}_m &= \mathbf{X}_m + \mathbf{u}_m, \\ \mathbf{x}_s &= \mathbf{X}_s + \mathbf{u}_s, \end{aligned}$$

where  $\mathbf{X}_m$  and  $\mathbf{X}_s$  are the position vectors for points at the initial configuration, and  $\mathbf{u}_m$  and  $\mathbf{u}_s$  are the displacement vectors.

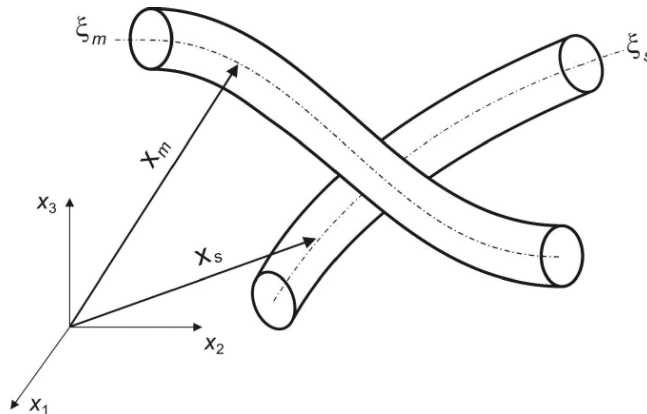


FIG. 1. Contacting beams.

For beams with a circular cross-section the closest points  $C_{mn}$  and  $C_{sn}$  are found on the curves representing the axes of the beams  $m$  and  $s$  (Fig. 2). The position vectors  $\mathbf{x}_{mn}$  and  $\mathbf{x}_{sn}$  of the closest points must simultaneously fulfil the orthogonality conditions between the connecting straight line and the lines tangent to curves at these points. If we assume that the symbol  $\circ$  defines the scalar product, then these conditions can be written as

$$(2.4) \quad \begin{cases} (\mathbf{x}_{mn} - \mathbf{x}_{sn}) \circ \mathbf{x}_{mn,m} = 0, \\ (\mathbf{x}_{mn} - \mathbf{x}_{sn}) \circ \mathbf{x}_{sn,s} = 0, \end{cases}$$

where

$$\mathbf{x}_{mn,m} = \frac{\partial \mathbf{x}_{mn}}{\partial \xi_m}, \quad \mathbf{x}_{sn,s} = \frac{\partial \mathbf{x}_{sn}}{\partial \xi_s}.$$

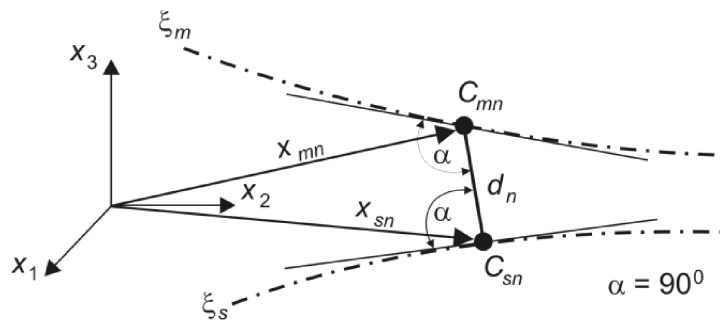


FIG. 2. The closest points on two curves.

Equations forming (2.4) are nonlinear functions of  $\xi_m$  and  $\xi_s$ . Their solution which defines the location of points  $C_{mn}$  and  $C_{sn}$ , can be obtained using the Newton-Raphson method. The linearization of Eq. (2.4) leads to two linear equations, which allow for calculation of the co-ordinate increments  $\Delta\xi_s$  and  $\Delta\xi_m$ :

$$(2.5) \quad \begin{bmatrix} \mathbf{x}_{m,m} \circ \mathbf{x}_{m,m} + (\mathbf{x}_m - \mathbf{x}_s) \circ \mathbf{x}_{m,mm} & -\mathbf{x}_{m,m} \circ \mathbf{x}_{s,s} \\ \mathbf{x}_{m,m} \circ \mathbf{x}_{s,s} & -\mathbf{x}_{s,s} \circ \mathbf{x}_{s,s} + (\mathbf{x}_m - \mathbf{x}_s) \circ \mathbf{x}_{s,ss} \end{bmatrix} \times \begin{bmatrix} \Delta\xi_m \\ \Delta\xi_s \end{bmatrix} = \begin{bmatrix} -(\mathbf{x}_m - \mathbf{x}_s) \circ \mathbf{x}_{m,m} \\ -(\mathbf{x}_m - \mathbf{x}_s) \circ \mathbf{x}_{s,s} \end{bmatrix}.$$

All the quantities in this formula must be determined for the current values of the co-ordinates  $\xi_m$  and  $\xi_s$ . The details for this linearization are given in the Appendix.

After finding the points  $C_{mn}$  and  $C_{sn}$ , the minimum distance between the beams can be found:

$$(2.6) \quad d_n = \|\mathbf{x}_{mn} - \mathbf{x}_{sn}\|.$$

### 2.3. Hertzian contact

To determine the value  $d$  present in (2.1) we can use results from Hertzian contact [4, 12], starting with an analysis of the contact between a rigid sphere and an elastic half-space (Fig. 3). For this case the normal force  $F$  is defined by:

$$(2.7) \quad F = \frac{4}{3} \cdot E \cdot R^{1/2} \cdot d^{3/2},$$

where  $E$  is the mean Young's modulus and  $R$  is the effective radius.

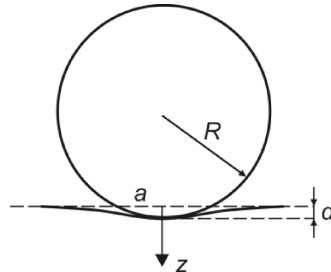


FIG. 3. A rigid sphere in contact with an elastic half-space.

The radius of the circular contact zone (Fig. 4) can be calculated as

$$(2.8) \quad a = \left( \frac{3 \cdot F \cdot R}{4 \cdot E} \right)^{1/3}.$$

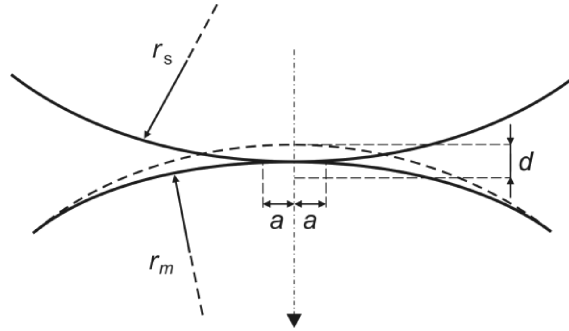


FIG. 4. The contraction of radii of contacting spheres.

The case of two identical cylinders with perpendicular axes representing two contacting beams leads to the same result as for a pair of spheres with radii  $r_s$  and  $r_m$  (Fig. 4). However, generally a contact zone between two cylinders has an elliptic shape. In this paper equations for a circular contact region are used with appropriate modifications. In Eq. (2.8) we use the value of the effective radius  $R$ , which is given by:

$$(2.9) \quad R = \sqrt{r_s \cdot r_m}.$$

If both bodies are elastic, then the following expression for the mean Young's modulus  $E$  can be used:

$$(2.10) \quad \frac{1}{E} = \frac{1 - \nu_s^2}{E_s} + \frac{1 - \nu_m^2}{E_m},$$

where  $E_s$  and  $E_m$  are the moduli of elasticity for both bodies, and  $\nu_s$  and  $\nu_m$  are the corresponding Poisson's ratios.

The normal force for the penalty method, which is a way to regularise the Signorini contact conditions, takes the following form:

$$(2.11) \quad F = \varepsilon_N \cdot g_N,$$

where  $\varepsilon_N$  is the penalty parameter and  $g_N$  is the value of penetration. The latter is defined in (2.1). The radii decrease  $d$  present in (2.1) is the only quantity which, at any iteration, is defined as independent of current displacements. Its value is determined as

$$(2.12) \quad d = \left( \frac{9}{16} \cdot \frac{\varepsilon_N^2 \cdot g_{Np}^2}{E^2 \cdot R} \right)^{1/3},$$

based on the value of the normal force and the normal gap  $g_{Np}$  evaluated in the previous iteration.

The penalty method used in the presented formulation has well known advantages and disadvantages. The price for its relative simplicity is the necessity to choose a suitable value for the penalty parameter  $\varepsilon_N$ . Care must be taken to keep it high enough to ensure good accuracy in fulfilling impenetrability conditions and, on the other hand, to keep it low enough to avoid parasitic numerical effects of the ill-posedness of the problem or contact and no contact oscillations, when the force resulting from (2.11) leads to opening of normal gaps.

#### 2.4. Friction model

In this paper the Coulomb model of dry friction with a constant friction coefficient  $\mu$  is used. The relation between the friction force  $F_T$  and normal force  $F_N$  in the contact zone for the slip state is defined by:

$$(2.13) \quad F_T = \mu \cdot F_N.$$

Advantage is taken from the analogy to a rigid-ideally plastic material as proposed in [10]. This makes it possible to distinguish between two states: the stick and the slip. The former is characterised by no relative displacement between the bodies, while for the latter relative displacement in the form of sliding is observed. For the beam-to-beam case two separate values of tangential displacement  $g_{Tm}$  and  $g_{Ts}$ , corresponding to two independent relative sliding movements on the beams  $m$  and  $s$ , must be introduced [8]. They are calculated as

$$(2.14) \quad g_{Tm} = g_{Tm}^e + g_{Tm}^p, \quad g_{Ts} = g_{Ts}^e + g_{Ts}^p,$$

where  $g_{Tm}^e$  and  $g_{Ts}^e$  are the stick components of displacements, and  $g_{Tm}^p$  and  $g_{Ts}^p$  are the slip components of displacements.

The values of stick components are used to define the components of the friction force. Using the penalty method, with a single tangential penalty parameter  $\varepsilon_T$  introduced, we obtain:

$$(2.15) \quad \begin{aligned} F_{Tm} &= \varepsilon_T \cdot g_{Tm}^e = \varepsilon_T (g_{Tm} - g_{Tm}^p), \\ F_{Ts} &= \varepsilon_T \cdot g_{Ts}^e = \varepsilon_T (g_{Ts} - g_{Ts}^p). \end{aligned}$$

The slip components of the tangential displacement can be obtained from the sliding rule:

$$(2.16) \quad \dot{g}_{Tm}^p = \dot{\gamma} \frac{\partial f_m}{\partial F_{Tm}}, \quad \dot{g}_{Ts}^p = \dot{\gamma} \frac{\partial f_s}{\partial F_{Ts}},$$

which corresponds to the non-associated flow rule in plasticity.

The gap increments in the step-wise analysis, used to integrate the sliding rule (2.16) with respect to time, are defined as straight-line distances between

the current contact points and mappings of the previous contact points onto the current beam configuration. The details can be found in [8].

For the Coulomb friction the sliding criterion is checked in the form:

$$(2.17) \quad f = \|\mathbf{F}_T\| - \mu F_N \leq 0.$$

The sign of the value of the sliding function (2.17) determines the current friction state. For non-positive values the stick state (elastic) is determined, for positive values the slip state (plastic) is determined. In the case of the slip state, the Euler procedure of return to the limit surface must be used.

The sliding rule has to be integrated with respect to a fictitious time. To this end, the incremental method can be applied. The trial values of the elastic displacement in the current step  $n$  are calculated as

$$(2.18) \quad g_{Tmn}^{et} = g_{Tmn} - g_{Tmp}^p, \quad g_{Tsn}^{et} = g_{Tsn} - g_{Tsp}^p,$$

where  $g_{Tmn}$  are the current values of total displacements and  $g_{Tmp}^p$  are the plastic parts of the tangential displacement from the previous step  $p$ .

The trial values of friction forces (2.15) are expressed as

$$(2.19) \quad F_{Tmn}^t = \varepsilon_T \cdot g_{Tmn}^{et}, \quad F_{Tsn}^t = \varepsilon_T \cdot g_{Tsn}^{et},$$

and are used to calculate the trial value of the friction force:

$$(2.20) \quad \|\mathbf{F}_T^t\| = F_T^t = \|F_{Tmn}^t \mathbf{t}_m + F_{Tsn}^t \mathbf{t}_s\|,$$

where  $\mathbf{t}_m$  and  $\mathbf{t}_s$  are the unit tangent vectors, see [8]. Using (2.19) in (2.20) the sliding limit function is checked. If the sliding criterion (2.17) is fulfilled, then the contact is in the stick state. In this case the real values of the friction forces are equal to their trial values:

$$(2.21) \quad F_{Tmn} = F_{Tmn}^t, \quad F_{Tsn} = F_{Tsn}^t,$$

and the plastic parts of the tangential displacements remain unchanged:

$$(2.22) \quad g_{Tmn}^p = g_{Tmp}^p, \quad g_{Tsn}^p = g_{Tsp}^p.$$

If the sliding function (2.20) is positive then the friction is in the slip state. In this case the resultant friction force is limited by the maximal value  $\mu F_N$  and can be determined from the relations:

$$(2.23) \quad F_{Tmn} = \mu \cdot p_m \cdot F_N, \quad F_{Tsn} = \mu \cdot p_s \cdot F_N,$$

where the proportion parameters, which also define the direction of sliding, are defined by:

$$(2.24) \quad p_m = \frac{F_{Tmn}^t}{F_T^t}, \quad p_s = \frac{F_{Tsn}^t}{F_T^t}.$$

The plastic parts of the tangential gaps (the sliding distances) are updated using

$$(2.25) \quad g_{Tmn}^p = g_{Tmn}^p + \frac{1}{\varepsilon_T} [F_{Tmn}^t - F_{Tmn} \text{sign}(g_{Tmn}^{et})],$$

$$g_{Tsn}^p = g_{Tsn}^p + \frac{1}{\varepsilon_T} [F_{Tsn}^t - F_{Tsn} \text{sign}(g_{Tsn}^{et})].$$

### 2.5. Weak form for frictional contact

In the theory of elasticity, the solution of a frictional contact problem for two bodies involves finding a minimum of the potential energy functional  $\Pi$ :

$$(2.26) \quad \min \Pi = \min (\Pi_1 + \Pi_2 + \Pi_c),$$

where  $\Pi_1$ ,  $\Pi_2$  are the potential energy of first and second body and  $\Pi_c$  is the energy resulting from contact.

The problem of low precision contact leads to a solution of the functional minimisation with inequality constraints. To solve this problem the concept of an active set is used. This procedure involves choosing the contact pairs which fulfil the condition  $g_N < 0$ . For these pairs the inequality constraints can be replaced by the equality constraints:

$$(2.27) \quad g_N = 0.$$

In this way the problem (2.26) takes the form of a functional minimisation with equality constraints which can be solved using, for instance, the penalty method. This leads to the following modification of the functional (2.26) subjected to the minimization:

$$(2.28) \quad \min \left( \Pi_1 + \Pi_2 + \sum_{act} \left( \frac{1}{2} \cdot \varepsilon_N \cdot g_N^2 + \frac{1}{2} \cdot \varepsilon_T \cdot g_T^2 \right) \right),$$

where the sum in (2.28) concerns all active contacting pairs of points. Components resulting from the contact and friction for all active constraints can be expressed in the following form:

$$(2.29) \quad \delta \Pi_c = \delta \Pi_{Tm} + \delta \Pi_{Ts} + \delta \Pi_{FN} = F_{Tmn} \delta g_{Tmn} + F_{Tsn} \delta g_{Tsn} + F_N \delta g_N.$$

Solution of the nonlinear problem in hand requires calculation of the linearization of the expression (2.29):

$$(2.30) \quad \Delta\delta\Pi_c = \Delta\delta\Pi_{T_m} + \Delta\delta\Pi_{T_s} + \Delta\delta\Pi_{F_N} = \Delta F_{T_{mn}}\delta g_{T_{mn}} + F_{T_{mn}}\Delta\delta g_{T_{mn}} \\ + \Delta F_{T_{sn}}\delta g_{T_{sn}} + \Delta F_{T_{sn}}\Delta\delta g_{T_{sn}} + \Delta F_N\delta g_N + F_N\Delta\delta g_N.$$

For the value of  $d$  written in (2.12) as

$$d = \left( \frac{9}{16} \cdot \frac{\varepsilon_N^2 \cdot g_{Np}^2}{E^2 \cdot R} \right)^{1/3},$$

the linearization and variation in the current step is zero  $\delta d = \Delta\delta d = 0$ . Therefore, the variation, linearization and second variation of the penetration function  $\delta g_n$ ,  $\Delta g_n$ ,  $\Delta\delta g_n$  can be obtained as in the analysis without the cross-section deformation [5]. Also the kinematic variables for friction at the contact points are computed in the same way, as in the analysis without the cross-section deformation [8] and thus are not given here.

### 3. NUMERICAL EXAMPLES

#### 3.1. Introduction

In this section three examples of beam-to-beam contact are presented. Each beam is discretised using ten identical co-rotational finite elements proposed in [1]. The curves representing beam axes are defined using Hermite's polynomials [8].

Let it also be noted, that the addition of Hertz contact results to the presented computational formulation of beam-to-beam contact does not significantly influence the convergence of the iterative process and its sensitivity to the values of penalty regularising parameters or the number of beam elements. To illustrate this a comparison of convergence behaviour is included in one of the examples. However, the examples mainly consider the influence of Hertzian results introduced to the normal contact definition on the numerical results such as values of penetration and tangential gaps for different scenarios.

#### 3.2. Example 1

Contact between two clamped-clamped beams is considered. The initial configuration of beam axes is shown in Fig. 5. The beams have circular cross-sections with radius  $r = 0.1$ , length 6.0 and are initially spaced at 0.001. They are made of a material with Young's modulus  $E = 250 \cdot 10^5$  and Poisson's ratio  $\nu = 0.3$ .

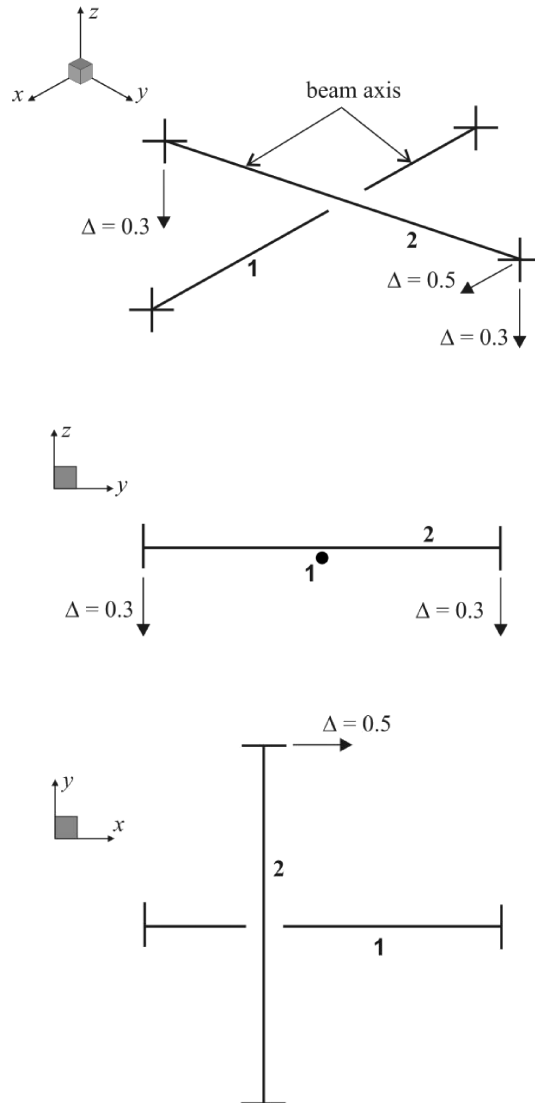


FIG. 5. The initial configuration of beam axes in Example 1.

The penalty parameters used in the analysis are  $\varepsilon_N = 1 \cdot 10^5$ ,  $\varepsilon_{T_m} = \varepsilon_{T_s} = 1 \cdot 10^3$  and the three values of the friction coefficient are  $\mu = 0, 0.2$  and  $0.5$ . The imposed displacements have the values  $\Delta = 0.3$  and  $0.5$  and are shown in Fig. 5. They are applied simultaneously in 60 equal increments.

The values of penetration of beams for different values of friction coefficient are presented in the tables below. In Table 1 for value of friction coefficient  $\mu = 0$ , in Table 2 for  $\mu = 0.2$  and in Table 3 for  $\mu = 0.5$ . In the second column

**Table 1.** Values of penetration for  $\mu = 0$  in Example 1.

Increment number	Penetration with $d$ $g_N = d_n - r_m - r_s + d$	Penetration without $d$ $g_N = d_n - r_m - r_s$	Value of $d$
10	0.0005332783	0.0005378782	0.000407326
20	0.0011724902	0.0011818589	0.000712649
30	0.0019863092	0.0020027648	0.001023030
40	0.0030404399	0.0030677971	0.001365500
50	0.0043953891	0.0044389864	0.001751300
60	0.006106108	0.0061728780	0.002185520

**Table 2.** Values of penetration for  $\mu = 0.2$  in Example 1.

Increment number	Penetration with $d$ $g_N = d_n - r_m - r_s + d$	Penetration without $d$ $g_N = d_n - r_m - r_s$	Value of $d$
10	0.0005305331	0.0005350921	0.000405899
20	0.0011677512	0.0011770592	0.000710672
30	0.0019804533	0.0019968380	0.001020930
40	0.0030348156	0.0030621312	0.001363720
50	0.0043914375	0.0044350533	0.001750150
60	0.0061055776	0.0061724790	0.002185290

**Table 3.** Values of penetration for  $\mu = 0.5$  in Example 1.

Increment number	Penetration with $d$ $g_N = d_n - r_m - r_s + d$	Penetration without $d$ $g_N = d_n - r_m - r_s$	Value of $d$
10	0.0005275242	0.0005320897	0.000404308
20	0.0011647286	0.0011740602	0.000709295
30	0.0019803911	0.0019968373	0.001020800
40	0.0030389499	0.0030663500	0.001364860
50	0.0043999527	0.0044436610	0.001793730
60	0.0061172561	0.0061842081	0.002188100

of the tables the values of the penetration with cross-section deformations taken into account are given and in the third column without deformations. In the last column the value of  $d$  is presented. The graphs presented in Figs. 7, 8, 9 and 10 show the evolution of the elastic and plastic parts of the tangential gaps for both beams. The deformed configuration of the axes of the beams is presented in Fig. 6.

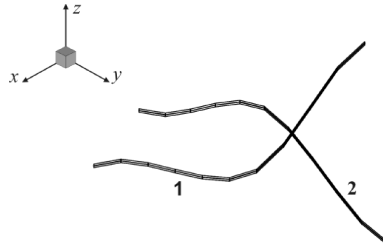


FIG. 6. Deformed configuration of beam axes in Example 1.

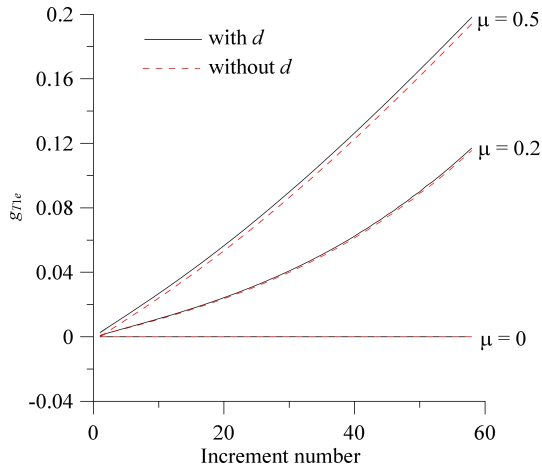


FIG. 7. Elastic parts of tangential gaps  $g_{T1e}$  on beam 1 in Example 1.

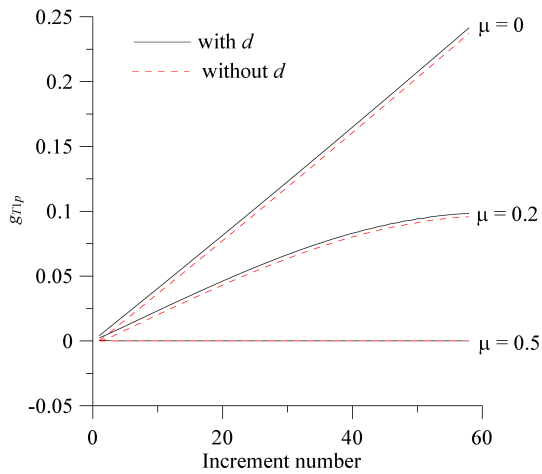


FIG. 8. Plastic parts of tangential gaps  $g_{T1p}$  on beam 1 in Example 1.

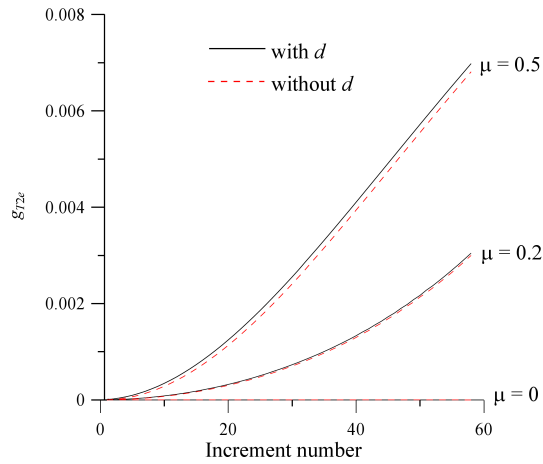


FIG. 9. Elastic parts of tangential gaps  $g_{T2e}$  on beam 2 in Example 1.

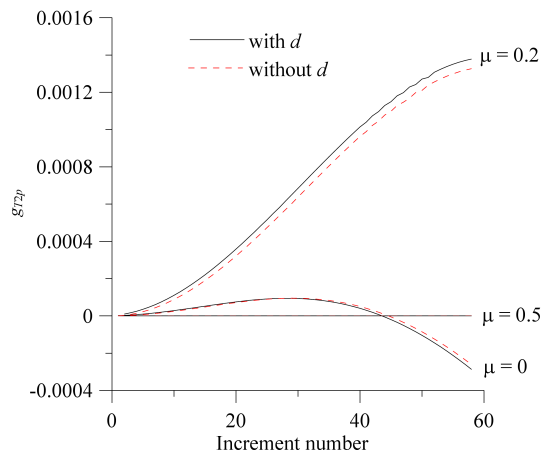


FIG. 10. Plastic parts of tangential gaps  $g_{T2p}$  on beam 2 in Example 1.

In this case for  $\mu = 0.5$  the friction in contact on both beams is in the stick state, while for the other values of the friction coefficient it is in the slip state.

The influence of the Hertz results applied to improve the physical law in the beam-to-beam contact interface is visible in the solution. In this example it reaches a few percent of the calculated values of normal and tangential gaps.

Interesting to note is the influence of the value of the friction parameter  $\mu$  on the results. It is clear in the case of dominant sliding along beam 1 that the in-

creasing value of  $\mu$  leads to less sliding. However, the much smaller “transverse” sliding along beam 2 features a different behaviour, including also a change of sliding direction in the case of very small or zero values of the friction coefficient (Fig. 8).

The values of the relative energy norm, computed as the quadratic norm of vector of displacement increments related to its corresponding value from the first iteration in given increments, are shown in Table 4 for two selected increments. They confirm the fact that the quadratic convergence is not influenced by the addition of beam cross-section deformation effects to the contact formulation.

**Table 4.** Values of relative energy norm in Example 1 for  $\mu = 2$ .

Increment number	Iteration number	Energy norm without $d$	Energy norm with $d$
30	1	1	1
	2	$6.18 \cdot 10^{-5}$	$1.87 \cdot 10^{-4}$
	3	$7.07 \cdot 10^{-11}$	$2.32 \cdot 10^{-9}$
60	1	1	1
	2	$1.99 \cdot 10^{-3}$	$1.92 \cdot 10^{-3}$
	3	$1.33 \cdot 10^{-7}$	$5.07 \cdot 10^{-8}$
	4	$8.17 \cdot 10^{-15}$	$5.22 \cdot 10^{-15}$

Note that the iterations were terminated when the relative energy norm dropped below  $10^{-8}$ .

### 3.3. Example 2

In this example contact between two cantilever beams with different radii is analysed. The beams have circular cross-sections with radius  $r_1 = 0.1$  and  $r_2 = 0.15$ , length 6.0 and are initially spaced at 0.001. They are made of the same material with  $E = 250 \cdot 10^5$  and  $\nu = 0.3$ . The penalty parameters are  $\varepsilon_N = 6 \cdot 10^4$ ,  $\varepsilon_{Tm} = \varepsilon_{Ts} = 1 \cdot 10^3$  and the friction coefficients are  $\mu = 0$  and  $\mu = 0.5$ . The imposed displacements  $\Delta = 0.5$  and 0.2 are applied simultaneously in 60 equal increments. The initial configuration of beam axes is presented in Fig. 11.

In Tables 5 and 6 the values of the penetration and  $d$  are presented. The evolutions of the elastic and plastic parts of the tangential displacements are shown in Figs. 13, 14, 15 and 16. The deformed configuration of the axes of the beams is presented in Fig. 12. In this case for  $\mu = 0.5$  the friction is in the stick state and for  $\mu = 0.0$  in the slip state.

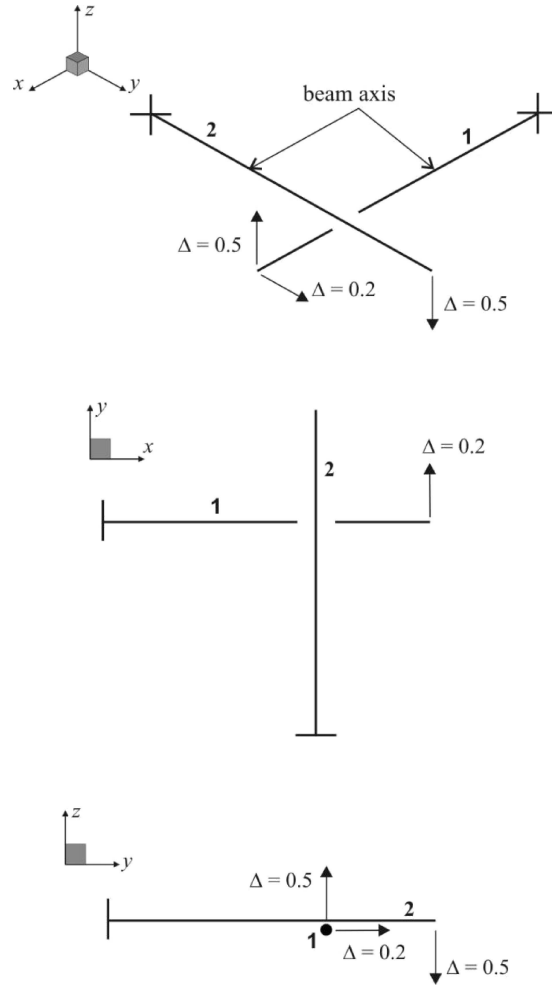


FIG. 11. The initial configuration of beam axes in Example 2.

**Table 5.** Values of penetration for  $\mu = 0$  in Example 2.

Increment number	Penetration with $d$ $g_N = d_n - r_m - r_s + d$	Penetration without $d$ $g_N = d_n - r_m - r_s$	Value of $d$
10	0.0067825603	0.0068080089	0.000319298
20	0.0137122930	0.0137543433	0.000530032
30	0.0205635086	0.0206189154	0.000702831
40	0.0273018797	0.0273690218	0.000854016
50	0.0339598676	0.0340382165	0.000991096
60	0.0406144977	0.0407043763	0.001119030

**Table 6.** Values of penetration for  $\mu = 0.5$  in Example 2.

Increment number	Penetration with $d$ $g_N = d_n - r_m - r_s + d$	Penetration without $d$ $g_N = d_n - r_m - r_s$	Value of $d$
10	0.0067959837	0.0068215218	0.000319662
20	0.0137998045	0.0138423928	0.000532083
30	0.0208358958	0.0208927021	0.000708670
40	0.0278788155	0.0279483907	0.000865562
50	0.0349241326	0.0350057636	0.001009330
60	0.0419935470	0.0420871265	0.001143880

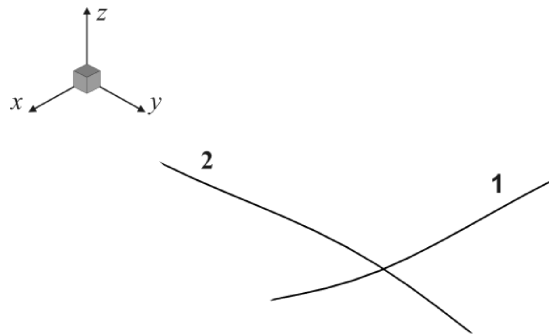


FIG. 12. Deformed configuration of beam axes in Example 2.

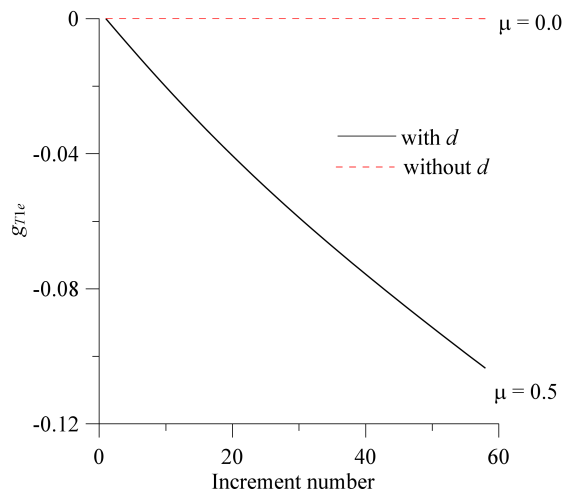


FIG. 13. Elastic parts of tangential gaps  $g_{T1e}$  on beam 1 in Example 2.

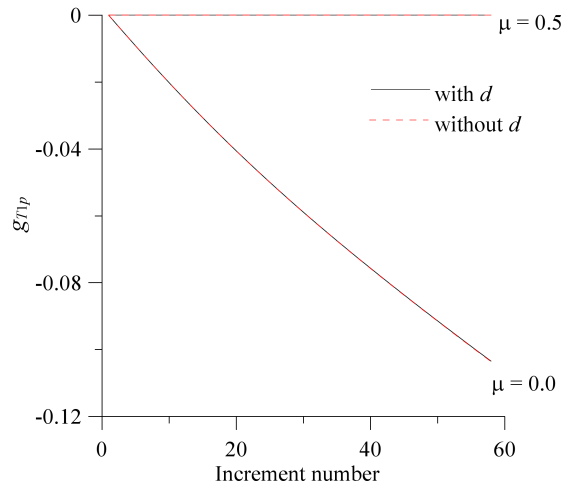


FIG. 14. Plastic parts of tangential gaps  $g_{T1p}$  on beam 1 in Example 2.

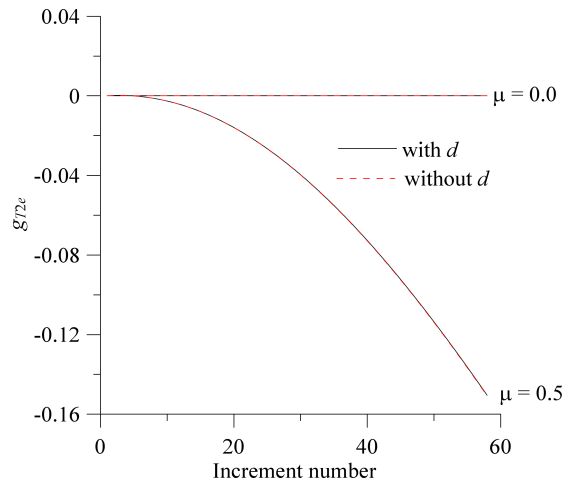


FIG. 15. Elastic parts of tangential gaps  $g_{T2e}$  on beam 2 in Example 2.

In this example the differences between the beam-to-beam contact formulation with Hertzian improvement of the contact interface law do not differ visibly from the original results with low-precision contact formulation from [8]. This influence is well below 1% in the calculated normal and tangential gaps.

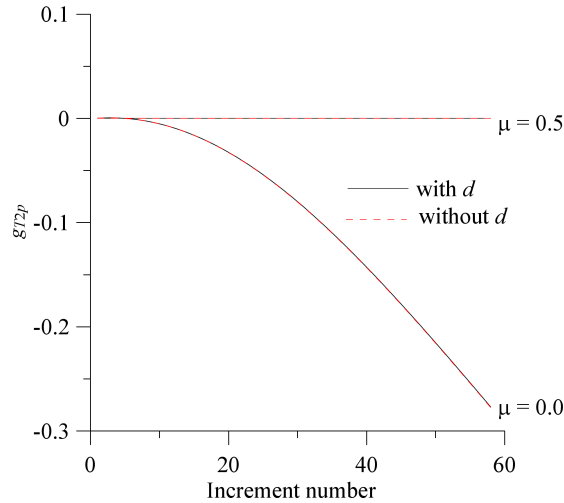


FIG. 16. Plastic parts of tangential gaps  $g_{T2p}$  on beam 2 in Example 2.

### 3.4. Example 3

In this example contact between four beams forming a symmetric assembly is considered. The axes of the beams in the initial configuration are presented in Fig. 17. Each of the beams has almost fully constrained centre points, except for the freedom of rotation about the axes in the plane perpendicular to the beams. The imposed displacements  $\Delta = 1.5$  are applied in 30 equal increments at free ends of the beams.

The beams have circular cross-sections with radius  $r = 0.1$ , length 8.0 and are initially spaced at 0.001. They are made of the same material with  $E = 250 \cdot 10^5$  and  $\nu = 0.3$ . The penalty parameters are  $\varepsilon_N = 4 \cdot 10^4$  and  $\varepsilon_{Tm} = \varepsilon_{Ts} = 7 \cdot 10^3$ , the friction coefficients are  $\mu = 0$  and  $\mu = 0.5$ .

The values of penetration of beams for two values of friction coefficient are presented in Tables 7 and 8. The graphs in Fig. 19 present the development of the total tangential displacement in the contact. In this case for  $\mu = 0.0$  the friction is in the slip state and the elastic part of total tangential displacement is zero. Thus the graph shown in Fig. 19 represents the plastic part of the gap only. Contrary to this, for  $\mu = 0.5$  the beams are in the stick state, the plastic part of tangential gaps is zero and the graph in the figure represents the elastic part.

Here, the inclusion of the Hertzian improvement in the contact interface law leads to a difference in the calculated normal and tangential gaps reaching 1%.

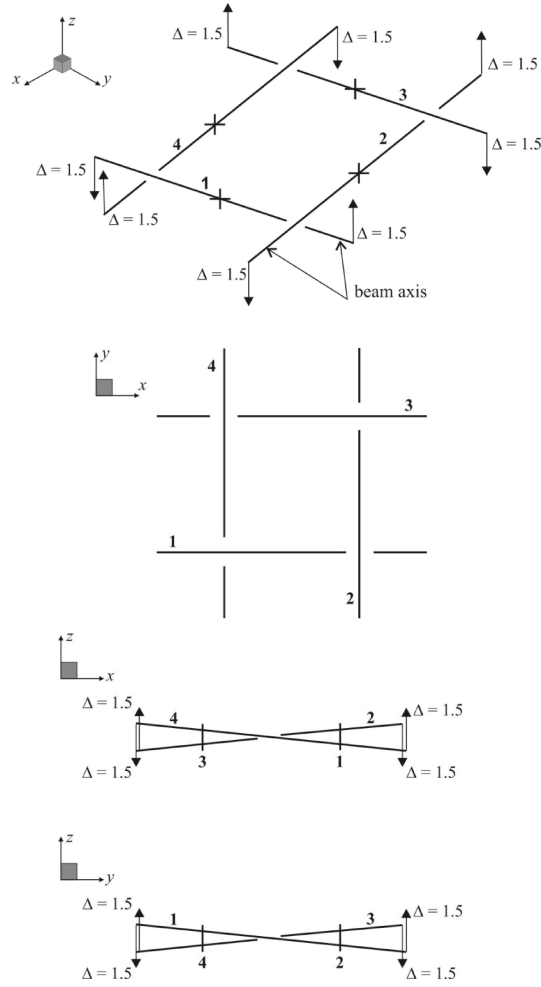


FIG. 17. The initial configuration of beam axes in Example 3.

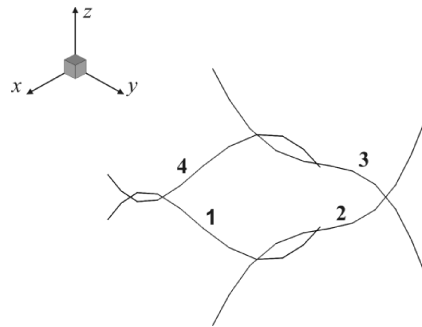


FIG. 18. Deformed configuration of beam axes in Example 3.

**Table 7.** Values of penetration for  $\mu = 0$  in Example 3.

Increment number	Penetration with $d$ $g_N = d_n - r_m - r_s + d$	Penetration without $d$ $g_N = d_n - r_m - r_s$	Value of $d$
5	0.0037954984	0.0038097636	0.000854052
10	0.0080798670	0.0081072371	0.001543900
15	0.0126966065	0.0127384916	0.002137810
20	0.0179055316	0.0179667837	0.002715300
25	0.0241296867	0.0242204171	0.003326000
30	0.0321341627	0.0322764809	0.004026210

**Table 8.** Values of penetration for  $\mu = 0.5$  in Example 3.

Increment number	Penetration with $d$ $g_N = d_n - r_m - r_s + d$	Penetration without $d$ $g_N = d_n - r_m - r_s$	Value of $d$
5	0.0038018158	0.0038161508	0.000855282
10	0.0080696636	0.0080970042	0.001543230
15	0.0126338143	0.0126753194	0.002131960
20	0.0177269233	0.0177872712	0.002699190
25	0.0237611000	0.0240861931	0.003294170
30	0.0315726000	0.0318330760	0.003978960

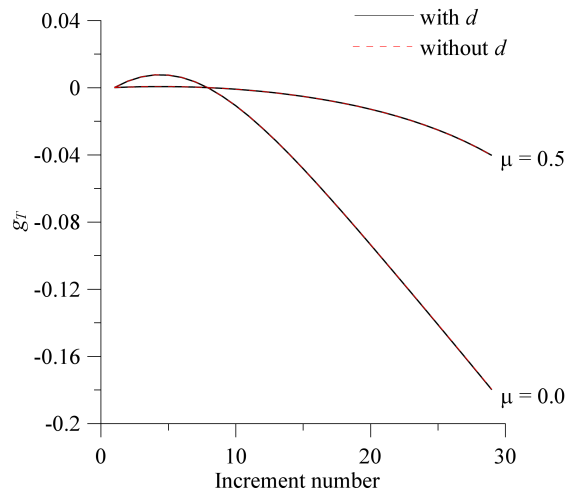


**FIG. 19.** Evolution of tangential displacements  $g_T$  in Example 3.

## 4. SUMMARY

A simple method to include the cross-section deformation in the analysis of beam-to-beam contact has been presented. The method uses a classical Hertz solution for two contacting cylinders. In this way the low precision contact model from [8] has been improved with introduction of the physical law for the contact interface interaction. The present formulation is the first step to achieve a realistic description of beam-to-beam contact taking into account the cross-section deformations at the contact zone.

Preliminary results for a few analysed examples indicate that the difference between the frictional contact forces evaluated either with or without this correction is generally in the range of 1–1.5%, however in several cases it may be up to 5%.

It is important from the computational practice that no noticeable differences in the computer time or convergence speed have been observed when compared with the unmodified formulation

Future work will include a possible application of more general contact interface models to determine the cross-section change, e.g. for beams with tangents forming arbitrary angles. It is our opinion that a generalisation of the Hertz result can be combined with the three-point approximation of linear contact zone [9] to correctly and efficiently model such contact cases.

APPENDIX. THE LINEARIZATION OF THE ORTHOGONALITY CONDITION  
USING NEWTON'S PROCEDUR

The orthogonality conditions between a connecting straight line and lines tangent to curves at the position vectors  $\mathbf{x}_{mn}$  and  $\mathbf{x}_{sn}$  are written as

$$(A.1) \quad \begin{cases} (\mathbf{x}_m - \mathbf{x}_s) \circ \mathbf{x}_{m,m} = 0, \\ (\mathbf{x}_m - \mathbf{x}_s) \circ \mathbf{x}_{s,s} = 0, \end{cases}$$

where the partial derivatives with respect to the local coordinates  $\xi_s$  and  $\xi_m$  were introduced:

$$\mathbf{x}_{m,m} = \frac{\partial \mathbf{x}_m}{\partial \xi_m}, \quad \mathbf{x}_{s,s} = \frac{\partial \mathbf{x}_s}{\partial \xi_s}.$$

In the calculations the following notation was introduced: the first equation of (A.1) is denoted as  $d_1$ , and the second as  $d_2$ :

$$(A.2) \quad \begin{aligned} d_1 &= \mathbf{x}_m \circ \mathbf{x}_{m,m} - \mathbf{x}_s \circ \mathbf{x}_{m,m} = 0, \\ d_2 &= \mathbf{x}_m \circ \mathbf{x}_{s,s} - \mathbf{x}_s \circ \mathbf{x}_{s,s} = 0. \end{aligned}$$

The linearization of functions (A.2) using the Newton method can be written as

$$(A.3) \quad \begin{aligned} d_{1n} &= d_{10} + \frac{\partial d_1}{\partial \xi_s} \Delta \xi_s + \frac{\partial d_1}{\partial \xi_m} \Delta \xi_m = 0, \\ d_{2n} &= d_{20} + \frac{\partial d_2}{\partial \xi_s} \Delta \xi_s + \frac{\partial d_2}{\partial \xi_m} \Delta \xi_m = 0, \end{aligned}$$

where

$$(A.4) \quad \begin{aligned} d_{10} &= \mathbf{x}_m \circ \mathbf{x}_{m,m} - \mathbf{x}_s \circ \mathbf{x}_{m,m}, \\ d_{20} &= \mathbf{x}_m \circ \mathbf{x}_{s,s} - \mathbf{x}_s \circ \mathbf{x}_{s,s}, \\ \frac{\partial d_1}{\partial \xi_m} &= \mathbf{x}_{m,m} \circ \mathbf{x}_{m,m} + \mathbf{x}_m \circ \mathbf{x}_{m,mm} - \mathbf{x}_{sn} \circ \mathbf{x}_{m,mm} \\ &= (\mathbf{x}_m - \mathbf{x}_s) \circ \mathbf{x}_{m,mm} + \mathbf{x}_{m,m} \circ \mathbf{x}_{m,m}, \\ \frac{\partial d_1}{\partial \xi_s} &= -\mathbf{x}_{sn,s} \circ \mathbf{x}_{mn,m}, \\ \frac{\partial d_2}{\partial \xi_s} &= \mathbf{x}_m \circ \mathbf{x}_{s,ss} - \mathbf{x}_{s,s} \circ \mathbf{x}_{s,s} - \mathbf{x}_s \circ \mathbf{x}_{s,ss} \\ &= (\mathbf{x}_m - \mathbf{x}_s) \circ \mathbf{x}_{s,ss} - \mathbf{x}_{s,s} \circ \mathbf{x}_{s,s}, \\ \frac{\partial d_2}{\partial \xi_m} &= \mathbf{x}_{m,m} \circ \mathbf{x}_{s,s}. \end{aligned}$$

Substitution of (A.4) and (A.2) into (A.3) yields:

$$(A.5) \quad \begin{aligned} d_{1n} &= \mathbf{x}_m \circ \mathbf{x}_{m,m} - \mathbf{x}_s \circ \mathbf{x}_{m,m} + (-\mathbf{x}_{s,s} \circ \mathbf{x}_{m,m}) \Delta \xi_s \\ &\quad + [(\mathbf{x}_m - \mathbf{x}_s) \circ \mathbf{x}_{m,mm} + \mathbf{x}_{m,m} \circ \mathbf{x}_{m,m}] \Delta \xi_m = 0, \\ d_{2n} &= \mathbf{x}_m \circ \mathbf{x}_{s,s} - \mathbf{x}_s \circ \mathbf{x}_{s,s} + [(\mathbf{x}_m - \mathbf{x}_s) \circ \mathbf{x}_{s,ss} - \mathbf{x}_{s,s} \circ \mathbf{x}_{s,s}] \Delta \xi_s \\ &\quad + (\mathbf{x}_{m,m} \circ \mathbf{x}_{s,s}) \Delta \xi_m = 0, \end{aligned}$$

leading to:

$$(A.6) \quad \begin{aligned} &(-\mathbf{x}_{s,s} \circ \mathbf{x}_{m,m}) \Delta \xi_s + [(\mathbf{x}_m - \mathbf{x}_s) \circ \mathbf{x}_{m,mm} + \mathbf{x}_{m,m} \circ \mathbf{x}_{m,m}] \Delta \xi_m \\ &= -(\mathbf{x}_m \circ \mathbf{x}_{m,m} - \mathbf{x}_s \circ \mathbf{x}_{m,m}), \\ &[(\mathbf{x}_m - \mathbf{x}_s) \circ \mathbf{x}_{s,ss} - \mathbf{x}_{s,s} \circ \mathbf{x}_{s,s}] \Delta \xi_s + (\mathbf{x}_{m,m} \circ \mathbf{x}_{s,s}) \Delta \xi_m \\ &= -(\mathbf{x}_m \circ \mathbf{x}_{s,s} - \mathbf{x}_s \circ \mathbf{x}_{s,s}). \end{aligned}$$

Now the linearization of (2.4) can be expressed as

$$(A.7) \quad \left\{ \begin{array}{l} (-\mathbf{x}_{s,s} \circ \mathbf{x}_{m,m}) \Delta \xi_s + [(\mathbf{x}_m - \mathbf{x}_s) \circ \mathbf{x}_{m,mm} + \mathbf{x}_{m,m} \circ \mathbf{x}_{m,m}] \Delta \xi_m \\ \qquad \qquad \qquad = -(\mathbf{x}_m \circ \mathbf{x}_{m,m} - \mathbf{x}_s \circ \mathbf{x}_{m,m}), \\ \\ [(\mathbf{x}_m - \mathbf{x}_s) \circ \mathbf{x}_{s,ss} - \mathbf{x}_{s,s} \circ \mathbf{x}_{s,s}] \Delta \xi_s + (\mathbf{x}_{m,m} \circ \mathbf{x}_{s,s}) \Delta \xi_m \\ \qquad \qquad \qquad = -(\mathbf{x}_m \circ \mathbf{x}_{s,s} - \mathbf{x}_s \circ \mathbf{x}_{s,s}), \end{array} \right.$$

or, finally, in the matrix form:

$$(A.8) \quad \begin{bmatrix} \mathbf{x}_{m,m} \circ \mathbf{x}_{m,m} + (\mathbf{x}_m - \mathbf{x}_s) \circ \mathbf{x}_{m,mm} & -\mathbf{x}_{s,s} \circ \mathbf{x}_{m,m} \\ \mathbf{x}_{m,m} \circ \mathbf{x}_{s,s} & (\mathbf{x}_m - \mathbf{x}_s) \circ \mathbf{x}_{s,ss} - \mathbf{x}_{s,s} \circ \mathbf{x}_{s,s} \end{bmatrix} \\ \times \begin{bmatrix} \Delta \xi_m \\ \Delta \xi_s \end{bmatrix} = \begin{bmatrix} -(\mathbf{x}_m - \mathbf{x}_s) \circ \mathbf{x}_{m,m} \\ -(\mathbf{x}_m - \mathbf{x}_s) \circ \mathbf{x}_{s,s} \end{bmatrix}.$$

#### ACKNOWLEDGMENT

This work was sponsored by the internal grants: DSMK 11-509/2015 and DSPB 11-400/2015.

#### REFERENCES

1. CRISFIELD M.A., *A consistent co-rotational formulation for non-linear, three-dimensional beam-elements*, Computer Methods in Applied Mechanics and Engineering, **81**, 2, 131–150, 1990.
2. DURVILLE D., *Numerical simulation of entangled materials mechanical properties*, Journal of Materials Science, **40**, 22, 5941–5948, 2005.
3. DURVILLE D., *Contact-friction modeling within elastic beam assemblies: an application to knot tightening*, Computational Mechanics, **49**, 6, 687–707, 2012.
4. JOHNSON K.L., *Contact mechanics*, 81–104, Cambridge University Press, Cambridge, 1985.
5. KAWA O., LITEWKA P., *Contact between 3-D beams with deformable circular cross-sections*, [in:] *Recent Advances in Computational Mechanics*, T. Lodygowski, J. Rakowski, P. Litewka [Eds.], pp. 183–190, CRC Press/Balkema, Taylor & Francis Group, London, 2014.
6. KONYUKHOV A., SCHWEIZERHOF K., *Geometrically exact covariant approach for contact between curves*, Computer Methods in Applied Mechanics and Engineering, **199**, 37–40, 2510–2531, 2010.
7. KONYUKHOV A., SCHWEIZERHOF K., *Computational contact mechanics. Geometrically exact theory for arbitrary shaped bodies*, Lecture Notes in Applied and Computational Mechanics, 67, Springer, Heidelberg, New York, Dordrecht, London, 2013.

8. LITEWKA P., *Finite element analysis of beam to beam contact*, Springer, Berlin, Heidelberg, 2010.
9. LITEWKA P., *Enhanced multiple-point beam-to-beam frictionless contact finite element*, Computational Mechanics, **52**, 6, 1365–1380, 2013.
10. MICHAŁOWSKI R., MRÓZ Z., *Associated and non-associated sliding rules in contact friction problems*, Archives of Mechanics, **30**, 3, 259–276, 1978.
11. PACZELT I., BELEZNAI R., *Nonlinear contact-theory for analysis of wire rope strand using high-order approximation in the FEM*, Computers and Structures, **89**, 11–12, 1004–1025, 2011.
12. POPOV V.L., *Contact Mechanics and Friction*, 55–64, Springer, Berlin, Heidelberg, 2010.
13. WRIGGERS P., ZAVARISE G., *On contact between three-dimensional beams undergoing large deflections*, Communications in Numerical Methods in Engineering, **13**, 6, 429–438, 1997.
14. ZAVARISE G., WRIGGERS P., *Contact with friction between beams in 3-D space*, International Journal for Numerical Methods in Engineering, **49**, 8, 977–1006, 2000.

*Received March 6, 2015; accepted version June 30, 2015.*

---